Journal of
Materials Chemistry A

Accepted Manuscript

This article can be cited before page numbers have been issued, to do this please use: C. Sun, Q. Xu, Y. Xie, Y. Ling and Y. hou, *J. Mater. Chem. A*, 2018, DOI: 10.1039/C7TA10274G.

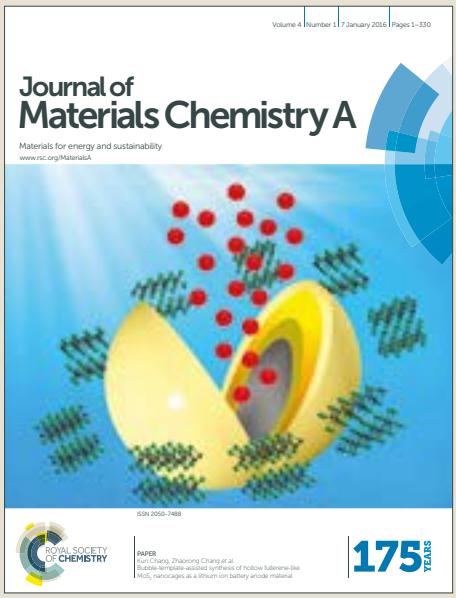

ROYAL SOCIETY OF CHEMISTRY

rsc.li/materials-a

View Article Online
DOI: 10.1039/C7TA10274G

Journal of Materials Chemistry A

ARTICLE

Designed synthesis of anatase-TiO_2 (B) biphase nanowires/ZnO nanoparticles heterojunction for enhanced photocatalysis

Received 00th January 20xx,
Accepted 00th January 20xx

DOI: 10.1039/x0xx00000x

www.rsc.org/

Chaoyang Sun,[a] Qiuhua Xu,[a] Yu Xie,*[,a] Yun Ling[a] and Yang Hou*[,b,c]

A high performance photocatalyst based on heterostructure using ZnO nanoparticles (NPs) decorating mesoporous anatase–TiO_2 (B) biphase TiO_2 nanowires (NWs) was synthesized by a facile water bath reflux method. The morphology, structure, and optical property of the prepared hybrid photocatalyst were well characterized. The results showed that the mesoporous biphase TiO_2 NWs consisted of TiO_2 (B) and anatase phase. When ZnO NPs was loaded on the surface of biphase TiO_2 NWs, a heterojunction was formed between TiO_2 NWs and ZnO NPs that could favor the separation of photogenerated electron-hole pairs. The TiO_2-ZnO heterojunction exhibited remarkably enhanced photocatalytic activity and excellent stability for both the dyes degradation and H_2 evolution compared with those of TiO_2 NWs. The heterojunction with a 20 wt.% ZnO content exhibited the highest photocatalytic activity and the reaction rate constant was about 4.2 and 1.3 times higher than that of TiO_2 NWs for dye degradation and H_2 evolution, respectively. The main active species were found to be O_2•- and •OH by electron paramagnetic resonance technique. This work may open a promising venue in producing highly-efficient heterojunction photocatalyst with special structure for large-scale environment and energy applications.

1. Introduction

Environmental pollution and clean energy have become the main factors that influence the global sustainable development.[1, 2] Many efforts are being taken to develop more green and effective technologies to address these issues. The utilization of semiconductors for applications in photocatalytic pollutant degradation and H_2 production from water splitting has received much attention due to advantages of clean, low-cost, and environmentally friendly operation.[3-5] Titanium dioxide (TiO_2), one of the most promising photocatalytic material, has attracted arising extensive and long lasting attention owing to its excellent photocatalytic performance, high chemical stability, non-toxicity, and low cost.[6, 7] Nevertheless, wide band-gap (3.2 eV) of TiO_2 makes it only respond to ultraviolet light that accounts for only around 5% of the solar spectrum.[8, 9] Meanwhile, the recombination of photogenerated electron-hole pairs is another reason for the decrease in photocatalytic efficiency.[10] To date, various strategies have been developed to improve the photocatalytic performance of TiO_2, including doping TiO_2 with metal[11-13] and non-metal elements,[14-17] coupling with other semiconductors,[18-22] and surface sensitization,[23] etc. Among them, coupling photocatalyst with metal oxides such as CuO,[24] ZnO,[25] and NiO[26] has been demonstrated to be an effective approach to promote the separation efficiency of photoelectrons from vacancies, and thus enhance the overall photocatalytic activity.[27]

Recently, ZnO has been reported to be a promising optical and electronic material due to its wide band-gap of 3.37 eV and large exciton binding energy of 60 meV,[28] and widely used in the fields of photocatalysts, rechargeable lithium-ion batteries, gas sensors, and electrodes in solar cells.[29-32] Besides the similar band edge energy with TiO_2, ZnO possesses some distinctive advantages such as longer life time of photogenerated carriers, higher quantum yield, and higher electron mobility than that of TiO_2,[33, 34] which are favorable for the enhancement of photocatalytic activity. In addition, the properties of easy crystallization and anisotropic growth allow ZnO to be synthesized in a variety of nanostructures.[35] Importantly, the valence band position and energetic conduction of ZnO are favorable for the H_2 evolution from water splitting, and the band level of ZnO matches well with TiO_2.[36] Therefore, it is a promising way to enhance the photocatalytic performance for pollutant degradation and H_2 production by coupling ZnO with nanostructured TiO_2.

Since Iijima et al.[37] discovered carbon nanotubes in 1991, one dimensional (1D) nanomaterials, such as nanowires (NWs), nanotubes, nanorods, and nanofibers, have attracted much attention due to their distinctive advantages. TiO_2 NWs have a high aspect ratio with a length reaching hundreds of micrometers, which make it suitable to possess a relatively

[a] Nanchang Hangkong University, Department of Material Chemistry, Nanchang, Jiangxi Province, China. *E-mail: xieyu_121@163.com
[b] Key Laboratory of Biomass Chemical Engineering of Ministry of Education, College of Chemical and Biological Engineering, Zhejiang University, Hangzhou 310027, China. *E-mail: yhou@zju.edu.cn
[c] Department of Chemistry and Food Chemistry & Center for Advancing Electronics, Dresden (CFAED), Technische Universitaet Dresden, 01062 Dresden, Germany.
† Electronic Supplementary Information (SI) available. See DOI: 10.1039/x0xx00000x

large specific surface area and easy transfer of photogenerated electrons along the axial direction.[38] Furthermore, the advantages of TiO_2 NWs, such as higher chemical stability and lower photogenerated carrier recombination rate than those of TiO_2 nanoparticles (NPs), make it widely used in photodegradation and photocatalytic H_2 evolution from water splitting.[39, 40] Therefore, it is believed that the TiO_2 NWs coupled with ZnO to form a heterojunction will possess excellent photocatalytic properties.

Anatase, rutile, and brookite are the most common phases of TiO_2, which play important roles in photocatalytic activity. The TiO_2 (B) phase, discovered in late 1980s by Marchand et al.,[41] is a metastable phase with a loose structure and a lower density than that of anatase and rutile. During the past few decades, TiO_2 (B) has attracted much interest in the applications of rechargeable lithium-ion storage, sensor, and photocatalysis.[42, 43] Shen et al.[44] found that the formed Ti^{3+} and oxygen vacancies in TiO_2 (B) can enhance solar light absorption, thus improving the photocatalytic properties. Moreover, compared with single phase TiO_2, mixed phase TiO_2 can exhibit much higher photocatalytic activity than either of the component. For example, the commercial P25 (Degussa) that consists of anatase (~80%) and rutile (~20%), possesses higher photocatalytic activity than that of pure anatase or rutile,[45] which may be due to the fast interfacial electron transfer caused by difference between the conduction band edges of two phases, thus increasing charge separation efficiency. Although the photocatalytic activity of TiO_2 (B) is much lower than that of anatase, the existence of difference between anatase and TiO_2 (B) can improve the charge separation efficiency when the two phases are in contact with each other.[46, 47] It has been well established in the literatures that TiO_2 photocatalyst with the mixed phase of anatase and TiO_2 (B) exhibited superior photoactivity as compared to pure anatase and TiO_2 (B) catalyst.[43, 46, 47] Therefore, the construction of ZnO/biphase TiO_2 (B)/anatase heterojunction for pollutant degradation and H_2 evolution is actively being pursued.

In this work, a biphase anatase/TiO_2 (B) NWs was synthesized by a hydrothermal, ion exchange, and calcination of P25, and then the ZnO NPs was decorated on the biphase anatase/TiO_2 (B) NWs to form a TiO_2-ZnO heterojunction by a simple reflux method. The as-prepared hybrid photocatalyst exhibited a significant improvement in photocatalytic degradation and H_2 evolution from water splitting, thanks to the heterojunction formed at the interface of TiO_2-ZnO that reduced the recombination of photoinduced charge carriers, ultimately improving the photocatalytic efficiency.

2. Experimental

2.1. Materials preparation

Biphase TiO_2 NWs was prepared according to the precious reports with slight modifications.[48] All chemicals were of analytical grade and used without further purification. 2.0 g P25 (Beijing Entrepreneur Science & Trading Co., Ltd) was dispersed into 80 mL of 10 M NaOH (West Long Chemical Co., Ltd, purity > 96.0%) solution. After being ultrasonicated for 30 min, the mixture was kept under magnetic stirring for 30 min. Afterward, the mixture was transferred into a 100 mL Teflon-lined autoclave, which was further placed in an electric oven at 200 °C for 24 h. After naturally cooling in air, the product was harvested by centrifugation, and then washed with deionized water for several times until the pH of supernatant reached to 7.0. Then, the obtained precipitate was dispersed in 0.1 mol L^{-1} nitric acid (Cangzhou Longsheng Chemical Co., Ltd) solution with continuous stirring for 5 h. After that, the product was collected via centrifugation, and washed with deionized water, and then dried in a vacuum oven at 80 °C for 24 h. Finally, the obtained sample was calcined at 500 °C for 3 h with a heating rate of 5 °C min^{-1}.

ZnO NPs loaded biphase TiO_2 NWs heterojunction was synthesized by a reflux method. Typically, a certain amount of TiO_2 NWs was dispersed in 62.5 mL of 0.01 M $Zn(CH_3COO)_2$/methanol solution. After vigorous stirring, the mixture was kept under ultrasonic treatment for 30 min to obtain the uniform solution. Next, 32.5 mL of 0.03 M NaOH was added into the solution with strong stirring, followed by reflux at 6 h in 60 °C. Subsequently, the sample was collected by centrifugation, washed with deionized water and methanol, and then dried in a vacuum oven at 80 °C for 24 h. The weight percentages of ZnO in the hybrid photocatalysts were 0, 10, 15, 20, 30, 50, and 70 wt.%, and the resulting samples were labeled as TiO_2-ZnO-x, where x = 0, 10, 15, 20, 30, 50, and 70, respectively.

2.2. Materials Characterization

X-ray diffraction (XRD) measurement of the products was recorded on a Rigaku RINT 2000 Advance X-ray diffractometer (Cu Kα radiation, λ=1.5406 Å). Raman spectra were obtained on a laser Raman spectrometer with a back-scattering configuration using an Ar^+ laser (20 mW, 532 nm) as excitation source. The morphology of the samples was examined with a JEOL JSM-6700F Field emission scanning electron microscopy (FESEM) in a secondary electron scattering mode at 15 kV. The morphology and lattice structure was characterized by a Tecnai G2F20 S-Twin instrument at an accelerating voltage of 200 kV. The UV-Vis absorption spectra of the samples were recorded using an Evolution 220 UV-Vis spectrophotometer (Thermo Fisher) from 200 to 800 nm, using $BaSO_4$ powder as the substrate. The Brunauer–Emmett–Teller (BET) surface area and pore structure of the samples were measured with a NOVA 2000e (Quantachrome). The surface composition and chemical state were analyzed by an ESCALAB MK II X-ray photoelectron spectrometer (XPS) with a Mg Kα (1253.6 eV) as the excitation source. All the binding energy values in the XPS spectra were calibrated using carbon contaminant (C 1s: 284.6 eV) as reference.

2.3. Photoelectrochemical (PEC) measurements

PEC measurements were carried out using a CHI 660D electrochemical workstation in a conventional three electrode system. The TiO_2 and ZnO/TiO_2 electrodes were employed as the working electrode. Ag/AgCl electrode and glassy carbon electrode served as the reference and counter electrodes, respectively. 0.5 M sodium sulfate was used as the electrolyte solution (pH = 7.0). A 300 W Xe lamp (PLS-SXE300, Perfect Light Company, Beijing, China) was utilized as the light source. To prepare the working electrode, 10 mg TiO_2 or ZnO/TiO_2 sample was dispersed into 1 mL deionized

View Article Online DOI: 10.1039/C7TA10274G

water, respectively. Then, the suspension was dip-coated onto the surface of fluorine tin oxide (FTO) glass substrates (2 cm × 2 cm), and dried at room temperature. Electrochemical impedance spectra (EIS) of the samples were obtained in a 0.1 M KCl solution.

2.4. Photocatalytic activity measurements

Photocatalytic activity of the samples was evaluated by degradation of MO, MB, RhB, and phenol. A 300 W Xe lamp (PLS-SXE300, Perfect Light Company, Beijing, China) was used as the light source. The light intensity was 100 mW cm^{-2}. The distance between light source and the surface of reaction solution was set at 15 cm. 10 mg of photocatalyst was dispersed in an aqueous solution of MO (50 mL, 10 mg L^{-1}), RhB (50 mL, 10 mg L^{-1}), MB (50 mL, 10 mg L^{-1}), respectively, and 50 mg of photocatalyst was dispersed in an aqueous solution of phenol (50 mL, 10 mg L^{-1}). Prior to the irradiation, the mixtures were magnetically stirred for 30 min in dark to reach the adsorption-desorption equilibrium between the samples and model pollutants. At a given time interval, aliquots (3 mL) of the solution were sampled and subsequently centrifuged to remove the photocatalysts. The concentration was monitored by measuring the maximum absorbance at 463 nm for MO, 554 nm for RhB, 664 nm for MB, and 269 nm for phenol through a UV-Vis spectrophotometer (UV-2550, Shimadzu, Japan).

Photocatalytic H_2 evolution tests were carried out in a double jacketed British purple glass reactor with a flat optical window at room temperature. The experiments were conducted by dispersing 50 mg of photocatalyst in an aqueous solution containing 72 mL of deionized water and 8 mL of methanol used as the sacrificial reagent. Prior to the reaction, the mixture was thoroughly stirred to ensure that the photocatalyst was well distributed into the solution. The system was completely vacuumed to remove CO_2 and O_2 dissolved in water. A 300 W Xeon-lamp was used as the light source. The H_2 evolution was measured using an on-line gas chromatography (GC) with the interval of 0.5 h each (Huaai GC9560, TCD, China).

3. Results and discussion

X-ray diffraction (XRD) analysis was conducted to investigate the crystalline structure of the resulted materials. Fig. 1 shows the XRD patterns of TiO_2 NWs and TiO_2-ZnO samples. The TiO_2 NWs are mainly composed of anatase and TiO_2 (B) phases. The strongest peak at around 25.2° and the other peaks at 37.8, 53.9, 55.1, 62.6° correspond to the (101), (004), (105), (211), and (204) crystal planes of anatase TiO_2 (JCPDS 21-1272), whereas the peaks at 14.2, 28.6, 29.7, 29.9, 33.2, 43.5, 44.5, and 48.4° match well with the (001), (002), (401), (111), (310), (003), (601), and (020) crystal planes of TiO_2 (B) (JCPDS 46-1237). After coupling with ZnO NPs, the characteristic peaks for TiO_2 NWs and ZnO NWs are observed. From Fig. 1b, the peaks at 31.7, 34.4, 36.2, 47.54, 56.5, and 67.9° can be indexed as the (100), (002), (101), (102), (110), and (112) diffraction planes of ZnO with a wurtzite structure (JCPDS 89-1397). It is clearly seen that the loading amount of ZnO NPs has a great influence on the composition of TiO_2 crystal phase. The phases of TiO_2 NWs are mainly composed of TiO_2 (B) and relatively few anatase. However, with an increase of loading amount of ZnO NPs, the peaks intensities of TiO_2 (B) decrease gradually. When the content of ZnO NPs is up to 20%, the peaks intensities of TiO_2 (B) become weakened obviously, and when the content of ZnO NPs exceeds 20%, the (001) plane of TiO_2 (B) is vanished.

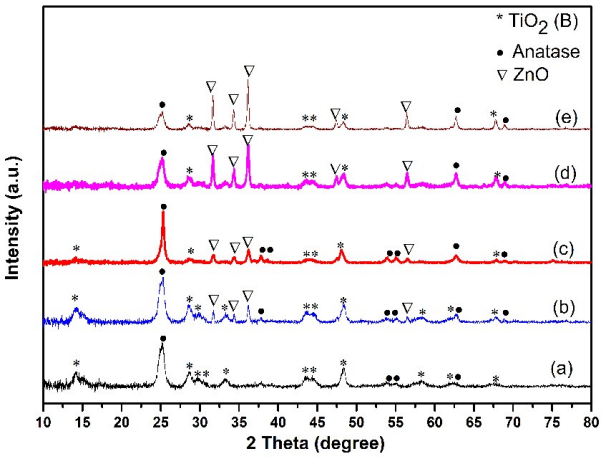

Fig. 1. XRD patterns of (a) TiO_2 NWs, (b) TiO_2-ZnO-10, (c) TiO_2-ZnO-20, (d) TiO_2-ZnO-30, and (e) TiO_2-ZnO-50.

Raman measurements were completed to further characterize the crystal structure of the TiO_2 NWs and TiO_2-ZnO samples. The Raman spectra of the TiO_2 NWs exhibit a small shift to the lower frequency compared with the previous results,[49, 50] which could mainly be attributed to the size effect and special nanostructure. For the TiO_2-ZnO samples, the peaks at 119, 236, and 248 cm^{-1} can be assigned to the vibration of TiO_2 (B), while the peaks at 141, 195, and 636 cm^{-1} are attributed to the Eg vibration of anatase (Fig. 2). No obvious ZnO peaks are observed in the hybrid. Raman analysis further confirms the presence of TiO_2 (B) and anatase, which are the main phases in the hybrid samples, consistent with the XRD results.

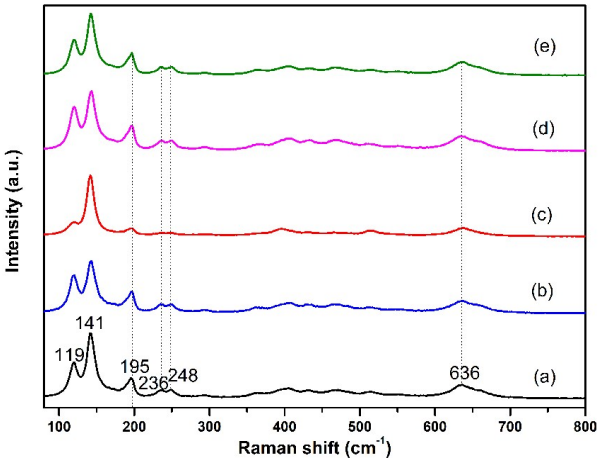

Fig. 2. Raman spectra of (a) TiO_2 NWs, (b) TiO_2-ZnO-10, (c) TiO_2-ZnO-20, (d) TiO_2-ZnO-30, and (e) TiO_2-ZnO-50.

FESEM measurements were conducted to investigate the surface morphologies of TiO_2 NWs and TiO_2-ZnO samples. The FESEM images in Fig. S1a shows that the TiO_2 NWs possess a typical 1D structure with a diameter of ~ 50 nm and a length of ~ 4 μm. Fig. S1b-e exhibit the morphology of ZnO NPs modified TiO_2 NWs with different loading amounts. It can be

View Article Online
DOI: 10.1039/C7TA10274G

clearly seen that the ZnO NPs is spherical nanoparticles with a diameter of ~ 20 nm, which is uniformly dispersed on the surface of TiO_2 NWs. For the TiO_2-ZnO-50 sample (Fig. S1d), most of the ZnO NPs were accumulated on the surface of TiO_2 NWs, which could lead to a decrease in photocatalytic activity. The energy-dispersive X-ray spectroscopy (EDS) and elemental mappings of the TiO_2-ZnO-20 sample prove the existence of Ti, O, and Zn elements in the hybrid (Fig. S1f-i).

TEM and high resolution TEM (HRTEM) measurements were conducted to investigate the microstructures of the TiO_2-ZnO-20 sample, and the results are shown in Fig. S2a-d. The TiO_2 NWs shows a uniform wire-like morphology with a rough surface; lots of ZnO NPs with a size of about 20 nm are attached on the surface of TiO_2 NWs. As shown in the HRTEM images (Fig. S2c-d), the lattice spacings of the TiO_2 NWs are 0.24, 0.35, and 0.38 nm, respectively, corresponding to the (001) and (101) crystal planes of anatase, as well as the (111) crystal plane of TiO_2 (B), which is well consistent with XRD results that the TiO_2 NWs was composed of TiO_2 (B) and anatase. The lattice spacing of ZnO NPs is about 0.26 nm, corresponding to the (002) plane of hexagonal wurtzite ZnO. The distinct and continuous fringe suggests the high crystallinity of the hybrid photocatalyst. Moreover, the circled zone in Fig. S2d shows that the interface between ZnO NPs and TiO_2 NWs is likely formed by epitaxial growth, which results in a strong interaction between ZnO and TiO_2. The strong interaction between them may be due to the fact that the lattice spacing of (101) plane for anatase is 0.35 nm which is close to the *a* and *b* values (*a* = *b* = 0.32 nm)[51] of the lattice parameters of hexagonal wurtzite ZnO. This match between the lattice parameters makes it easy to form a heterojunction between ZnO NPs and TiO_2 NWs.[52]

The optical properties of TiO_2 NWs and TiO_2-ZnO samples were investigated by UV-Vis diffuse reflectance spectroscopy (Fig. 3a). The absorption edge of TiO_2 NWs is estimated to be 470 nm. For the TiO_2-ZnO samples with different loading amounts, a slightly red shift of the absorption edges is observed compared with that of TiO_2 NWs. Thus, the TiO_2-ZnO samples can effectively extend the photo-responses of TiO_2 NWs into the visible spectrum, leading to the improvement of solar light utilization efficiency.

The band gap energies (Eg) are calculated from the Kubelka–Munk function plots of $(ah\nu)^{1/2}$ versus energy ($h\nu$) (Fig. 3b), where "a" and "$h\nu$" are the optical absorption coefficient and photonic energy, respectively. The E_g of TiO_2 NWs and TiO_2-ZnO-20 sample are determined to be 2.99 and 2.96 eV, respectively. The valence bands (VB) of TiO_2 NWs and TiO_2-ZnO-20 sample can be estimated by the following empirical equation:[53]

$$E_{VB} = X - Ee + 0.5\ Eg \quad (1)$$

$$E_{CB} = E_{VB} - Eg \quad (2)$$

X is the electronegativity of the semiconductor, and the value is 5.66 eV for TiO_2. Ee is the energy of free electron on the hydrogen scale (~ 4.5 eV), and Eg is the band gap energies of the semiconductor, which can be calculated to be 2.99 eV for the TiO_2. Thus, the E_{VB} of TiO_2 NWs and TiO_2-ZnO-20 sample are calculated to be 2.66 and 2.64 eV, and the E_{CB} of TiO_2 NWs and TiO_2-ZnO-20 sample are calculated to be -0.33 and -0.32 eV, respectively. Meanwhile, XPS valence spectra were used to determine the VB of TiO_2 NWs and TiO_2-ZnO-20 sample, and the results are shown in Fig. S3e-f. The TiO_2 NWs and TiO_2-ZnO-20 sample show the maximum energy edge of the VB at about 2.66 and 2.65 eV, respectively, which are consistent with the estimated values.

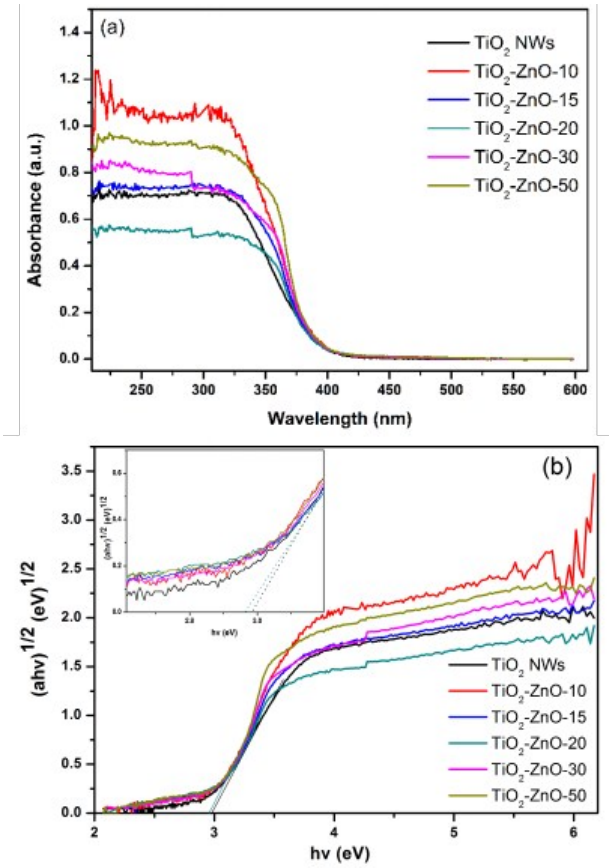

Fig. 3. (a) Optical absorption spectroscopy and (b) band gap of TiO_2 NWs, TiO_2-ZnO-10, TiO_2-ZnO-15, TiO_2-ZnO-20, TiO_2-ZnO-30, and TiO_2-ZnO-50.

XPS measurements were used to investigate the surface composition and the chemical state of the TiO_2 NWs and TiO_2-ZnO-20 sample. Fig. S3 shows the XPS survey spectra and high-resolution XPS spectra of Ti 2p, Zn 2p, and O 1s regions for the TiO_2-ZnO-20 sample. The survey spectra of the TiO_2 NWs and TiO_2-ZnO-20 sample further indicate the presence of Ti, Zn, O, and C elements in the TiO_2 NWs and TiO_2-ZnO-20 sample (Fig. S3a). Fig. S3b exhibits the high-resolution Ti 2p spectra of the TiO_2 NWs and TiO_2-ZnO-20 sample. In the Ti 2p spectra, the existence of Ti (IV) in the TiO_2-ZnO-20 sample is evidenced by a main peak located at 458.4 eV, slightly shifting of 0.1 eV towards the lower binding energy as compared to that of TiO_2 NWs (458.5 eV), which can be assigned to Ti $2p_{3/2}$. And the higher binding energy at 464.2 eV is assigned to Ti $2p_{1/2}$. The high-resolution Zn 2p spectra of the TiO_2-ZnO-20 sample (Fig. S3c) exhibit two contributions, Zn $2p_{1/2}$ and Zn $2p_{3/2}$, located at 1,021.5 and 1,044.6 eV, respectively, indicating that the Zn exists in the form of Zn^{2+}. The high-resolution O 1s spectra of the TiO_2-ZnO-20 sample in Fig. S3d can be fitted into two peaks. The main peak at 529.9 eV indicates that the O is in the form of O^{2-}. And the higher binding energy at 531.7 eV assigned to the -OH group on the surface of the TiO_2-ZnO-20 sample, shows an apparent shift of 0.2 eV towards the higher binding energy in contrast with that of TiO_2 NWs (531.5 eV).

View Article Online
DOI: 10.1039/C7TA10374C

The transient photocurrent tests were carried out to investigate the separation efficiency of the photogenerated electrons and holes pair of the as-prepared photocatalysts, and the results are shown in Fig. 4. For the TiO_2 NWs and TiO_2-ZnO samples, upon the light irradiation, the transient photocurrent is generated and then photocurrent density increases sharply. Subsequently, the photocurrent density decreases rapidly to zero when the irradiation is stopped. Clearly, the TiO_2-ZnO-20 sample exhibits the highest photocurrent density among all of the measured samples. The photocurrent density of 2.2 μA cm^{-2} for TiO_2-ZnO-20 sample was more than twice as high as that of the TiO_2 NWs (0.9 μA cm^{-2}). The enhanced photocurrent response of the TiO_2-ZnO-20 sample indicates that the coupling ZnO with TiO_2 is an efficient way to promote the separation of photogenerated electrons and holes.

EIS measurement was used to investigate the charge transfer resistance and the separation efficiency of the photo-generated electrons and holes. Fig. S4 shows the EIS Nynquist plots of TiO_2 NWs and TiO_2-ZnO samples before and after light irradiation. The arc radius of the TiO_2-ZnO-20 sample is the smallest among all of the samples under light irradiation, indicating that the TiO_2-ZnO-20 sample has the lowest electron-transfer resistance. The results demonstrate that the loading of ZnO NPs onto the surface of TiO_2 NWs can efficiently promote the separation of photogenerated charge carriers through an interfacial interaction between ZnO and TiO_2, which is an agreement with the transient photocurrent responses of these photocatalysts.

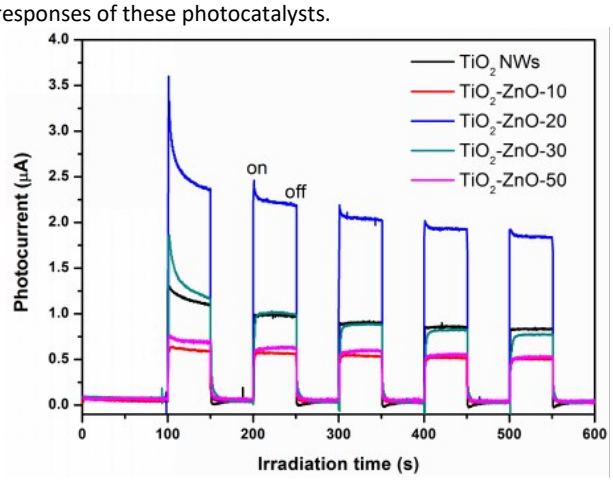

Fig. 4. Transient photocurrent responses of the TiO_2 NWs and TiO_2-ZnO samples.

Nitrogen physical adsorption was used to investigate the textural properties of the TiO_2 NWs and TiO_2-ZnO samples. The BET specific surface area, total pore volume, and average pore diameter of the TiO_2 NWs and TiO_2-ZnO samples are shown in Table S1. The BET specific surface area of TiO_2 NWs is calculated to be 21.94 $m^2 g^{-1}$, the average pore diameter and pore volume are 17.08 nm and 0.094 $cm^3 g^{-1}$, respectively. When the ZnO NPs are introduced onto TiO_2 NWs, the BET specific surface area firstly increases to 23.29 $m^2 g^{-1}$ for the TiO_2-ZnO-20 sample, and then decreases to 22.16 $m^2 g^{-1}$ with further increasing the loading amount of ZnO NPs to 50 wt.%, which can be attributed to the fact that a partial reunion phenomenon is occurred when the loading excessive ZnO NPs on the surface of TiO_2 NWs.[54] The agglomeration causes the decrease in BET specific surface area of hybrid photocatalysts. Among all of the samples, the TiO_2-ZnO-20 sample with the highest BET specific surface area is the most suitable candidate for photocatalytic reaction. The Nitrogen adsorption-desorption isotherms and pore size distributions of the TiO_2 NWs and TiO_2-ZnO samples are shown in Fig. 5. In Fig. 5a, the TiO_2 NWs shows a typical type-IV isotherm with a type H3 hysteresis loop at high relative pressure (P/P_0 = 0.6-1.0), suggesting the existence of mesoporous structure. The samples of TiO_2-ZnO-20 and TiO_2-ZnO-50 display similar isotherms as the TiO_2 NWs, indicating that the ZnO NPs loaded on the TiO_2 NWs has a minor impact on the mesoporous structure of TiO_2 NWs. The corresponding pore size distribution curves are shown in Fig. 5b. The pore size distribution curve of the TiO_2-ZnO-20 sample shows a broad peak, indicating the existence of different grades of porous structure, including the small mesopores of 10 nm and large mesopores of 20 nm, which are consistent with the TEM analysis. These different grades of porous structure are mainly originated from the nonuniform space between the packed NPs and existence of mesopores with different sizes on the surface of TiO_2 NWs. Such a hierarchical porous structure and high specific surface area of the TiO_2-ZnO hybrid can not only increase the contact area of the reactant molecules and catalyst surface, but also provide more favorable reaction sites in the process of adsorption and photocatalytic reaction, thus improving photocatalytic efficiency.

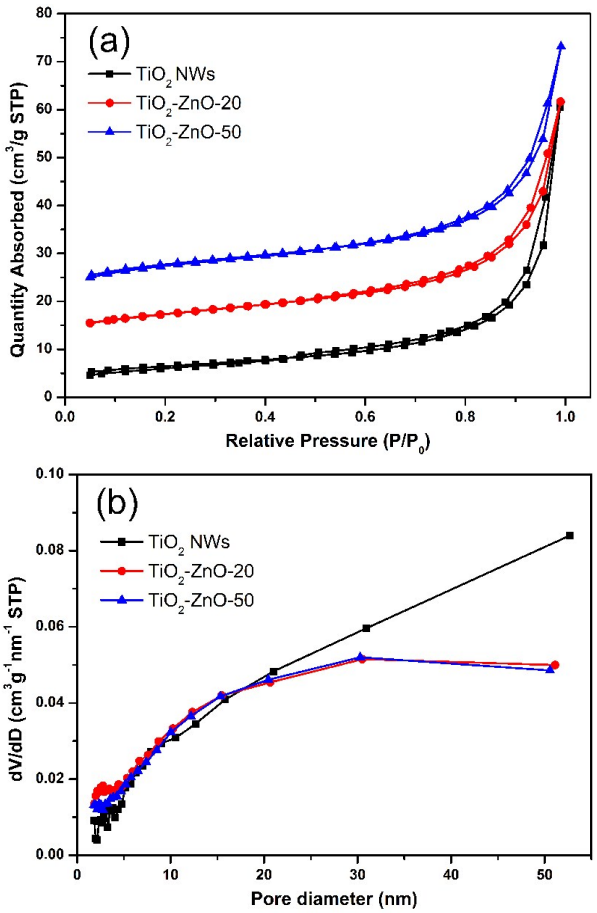

Fig. 5. Nitrogen adsorption–desorption isotherm of the TiO_2-ZnO samples with different loading amounts (a) and the corresponding pore size distributions curves (b).

The photocatalytic performance of TiO_2-ZnO samples was evaluated by the degradation of MO, as shown in Fig. 6a. There is almost no degradation of MO after 80 min irradiation in the absence of

View Article Online
DOI: 10.1039/C7TA10274G

photocatalyst, indicating that the MO molecules are sufficiently stable under UV-Vis light irradiation and its self-photolysis can be ignored in the photocatalytic process. 79.6% of MO is degraded over the pristine ZnO NPs after 50 min irradiation. And this percentage is further increased to be 97.7% over the TiO_2-ZnO-20 sample. As for the TiO_2 NWs, it shows a weak photocatalytic activity, and ~ 31% of MO is decomposed after 80 min irradiation. After coupling with ZnO NPs, the photocatalytic activity of TiO_2-ZnO hybrids firstly increases monotonously with the mass ratio of ZnO NPs increases from 10 wt.% to 20 wt.%, and then decreases with further increase of ZnO NPs content. Therefore, the 20 wt.% ZnO content in the TiO_2-ZnO samples is found to be the best loading ratio for MO degradation. The result suggests that the heterojunctions should be formed between ZnO NPs and TiO_2 NWs, which play crucial role in the separation and transfer of photo-generated charge carriers. Under the UV-Vis light irradiation, the generated electrons in the TiO_2 NWs and ZnO NPs could be excited from the valence band (VB) to the conduction band (CB). Due to the difference of CBs, the photo-generated electrons in the CB of anatase and ZnO can easily transfer to the TiO_2 (B), resulting in the efficient separation and reduced possibility of the recombination of photogenerated electron-hole pairs.

To better compare the photocatalytic performance of these samples, the reaction kinetics of MO degradation is investigated. Fig. 6b presents the linear fitting of the degradation time against $-\ln(C/C_0)$, and the reaction rate constants (k) are given in Table S2. Obviously, the degradation process of MO follows the pseudo-first-order kinetics, and the TiO_2-ZnO-20 sample has the maximum k value of 0.0420 min^{-1}, which is almost 4.2 times as high as that of TiO_2 NWs.

To further investigate the degradation of dyes with different structures, RhB and MB were also used to evaluate the photocatalytic activity of the as-prepared TiO_2-ZnO samples. As shown in Fig. 7a-b, upon light irradiation, the concentration of RhB and MB decreases gradually as the reaction time increases. The TiO_2-ZnO-20 sample exhibits excellent photocatalytic performance for the degradation of RhB and MB than those of TiO_2 NWs. Considering the obvious structural difference of the three dyes, it turns out that the TiO_2-ZnO hybrid has the universal application on degradation of dyes.

For comparison, the phenol was selected as a different kind of model pollutant to further ascertain the photocatalytic performance of the TiO_2-ZnO samples. As shown in Fig. 7c, the TiO_2-ZnO-20 sample shows a much higher photocatalytic performance than that of TiO_2 NWs. Fig. 7d exhibits a temporal evolution of the UV-Vis absorption of phenol solution degraded by the TiO_2-ZnO-20 sample. The intensity of the characteristic absorption peak at about 269 nm decreases gradually and about 99% phenol is degraded over TiO_2-ZnO-20 sample after 2 h irradiation. Based on this result, it can be reasonable to conclude that the MO, MB, and RhB degradation over TiO_2-ZnO samples are mainly attributed to the photocatalysis process of TiO_2-ZnO samples rather than the photosensitization effect of the dyes.

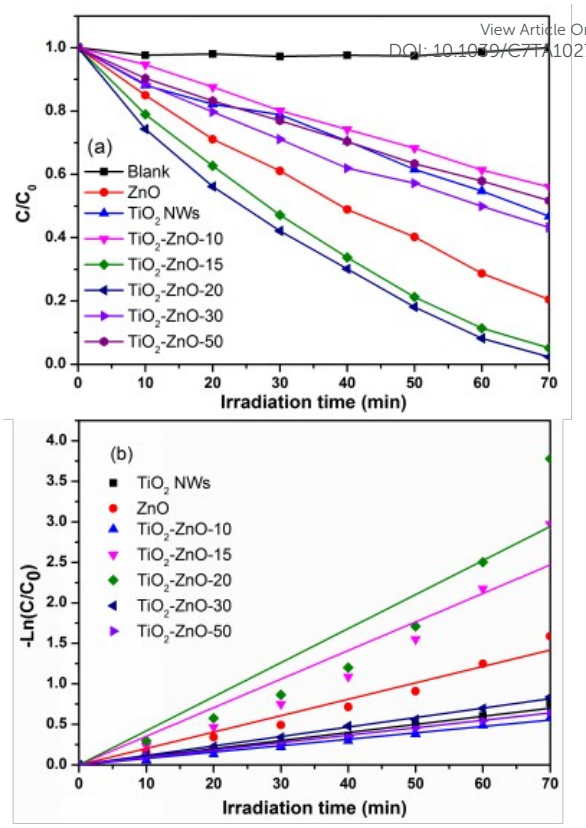

Fig. 6. (a) Photocatalytic degradation of MO in the presence of TiO_2 NWs and TiO_2-ZnO samples, and (b) kinetic fit for the degradation of MO with the TiO_2 NWs and TiO_2-ZnO samples.

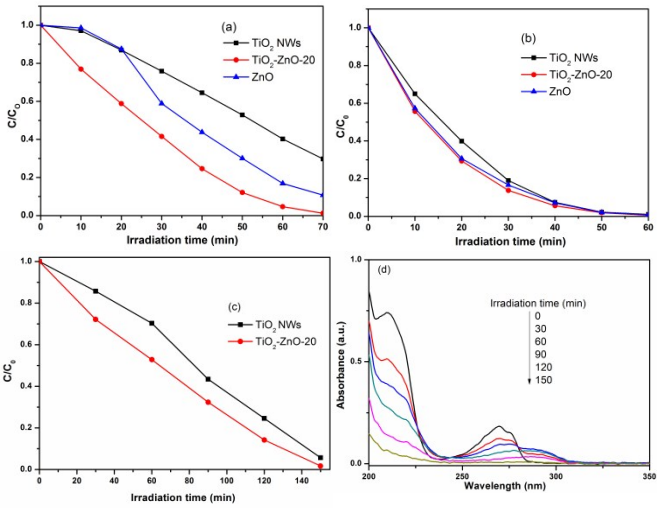

Fig. 7. Photocatalytic degradation of RhB (a), MB (b), and phenol (c) in the presence of TiO_2 NWs and TiO_2-ZnO-20 sample under light irradiation. (d) UV-Vis absorption spectral changes during the photocatalytic degradation of phenol in aqueous solution in the presence of the TiO_2-ZnO-20 sample.

In order to identify the active species over the TiO_2-ZnO samples, the EPR spin-trap experiments with 5,5-dimethyl-1-pyrroline *N*-oxide (DMPO) were carried out under light irradiation, and the results are shown in Fig. 8. The characteristic peaks from the DMPO-$O_2^{\bullet-}$ species can be observed in the dispersion of TiO_2-ZnO-20 sample, and the characteristic peaks of DMPO-$^{\bullet}$OH can also be

obviously observed in the irradiated suspension. The intensity of DMPO-$\cdot O_2^-$ signal is higher than that of DMPO-$\cdot$OH signal, which indicates that the $\cdot O_2^-$ radicals may play a more important role than $\cdot$OH radicals during the photodegradation process.

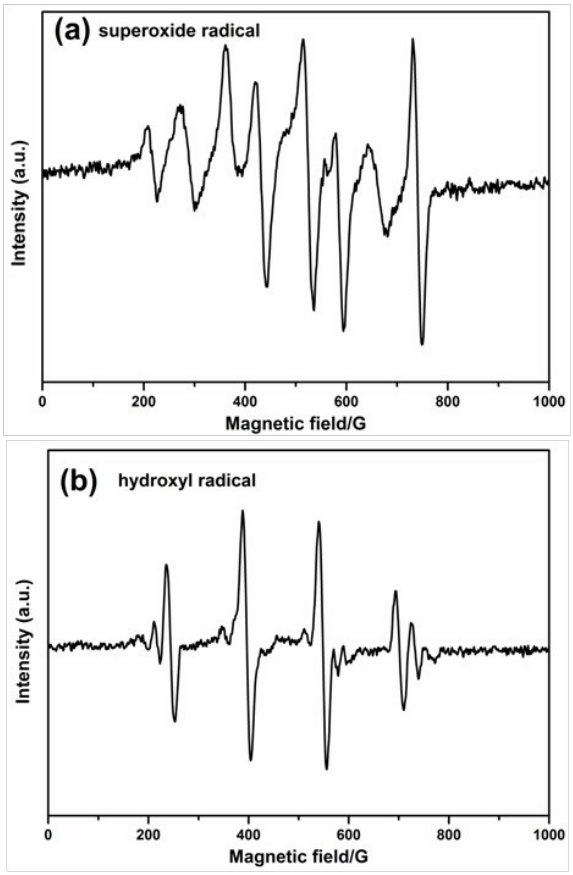

Fig. 8. EPR spectra of radical adducts trapped by DMPO in TiO_2-ZnO samples: (a) methanol dispersion and (b) aqueous dispersion under UV-Vis light irradiation.

In the photocatalytic reaction, the stability and repeatability of the photocatalyst are important factors affecting the photocatalytic efficiency. In order to get insights into the cycling stability, the TiO_2-ZnO-20 sample was used to test the recycling performance of photocatalyst. In our test, 60 mg of photocatalyst was added into the 30 mL of MO solution (10 mg L^{-1}), and then the mixture was magnetically stirred for 30 min in dark to reach the adsorption-desorption equilibrium between the powder sample and model pollutant. After 1 h light irradiation, the sample was collected by centrifugation and used for the next reaction. The experimental results are shown in Fig. 9. It is clear to see that the TiO_2-ZnO-20 sample still maintain the high activity even in the photocatalytic degradation experiment for 5 times. The results suggest that the structure of the as-prepared TiO_2-ZnO sample wis stable, reusable and hard to inactivate.

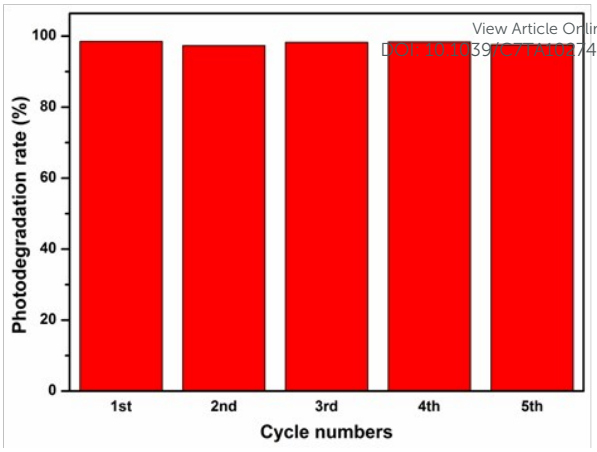

Fig. 9. Cycling performance of the TiO_2-ZnO-20 sample for MO degradation.

In order to further investigate the photocatalytic properties of as-prepared TiO_2-ZnO samples, additional experiments were carried out for photocatalytic H_2 evolution in the presence of 1 wt.% Pt co-catalyst. Fig. 10a shows the total H_2 evolution by TiO_2 NWs and the TiO_2-ZnO samples. The TiO_2-ZnO-20 sample displays the highest H_2 evolution among these samples at every 30 min. Fig. 10b shows the H_2 generation rate of TiO_2 NWs and all of the TiO_2-ZnO samples. The H_2 generation rate of the samples is relatively stable. The H_2 generation rate of the TiO_2 NWs, TiO_2-ZnO-10, TiO_2-ZnO-15, TiO_2-ZnO-20, TiO_2-ZnO-30, TiO_2-ZnO-50 samples are 145, 134, 181, 193 172, and 155 μmol h^{-1} g^{-1}, respectively. The results indicate that the TiO_2-ZnO-20 sample has the highest photocatalytic activity among these samples and its H_2 generation rate is about 1.3 times as much as that of TiO_2 NWs, revealing that the heterojunction structure is helpful to enhance the photocatalytic performance.

Based on the above results, a possible photocatalytic mechanism is proposed to explain the enhancement of the photocatalytic activity of TiO_2-ZnO heterostructure (Fig. 11). The TiO_2-ZnO photocatalyst is believed to exhibit cooperative or synergic effects among anatase, TiO_2 (B), and ZnO NPs. When the TiO_2-ZnO samples are irradiated by UV-Vis light, the photogenerated electrons in the VB of ZnO NPs and anatase–TiO_2 (B) biphase TiO_2 NWs can be excited to the CB of ZnO NPs and anatase–TiO_2 (B) biphase TiO_2 NWs, respectively. Then, the photogenerated electrons on the CB of ZnO NPs and TiO_2 (B) are transferred to the CB of anatase,[46] while the holes are transferred from the anatase and TiO_2 (B) to ZnO NPs due to the existence of energy gradient at the interface between ZnO, anatase, and TiO_2 (B). This process results in an effective separation of active photogenerated electrons and holes, thus increasing the lifetime of the charge carriers and hence improving the photocatalytic activity. The separated photogenerated electrons can reduce the H_2O to H_2, and the holes can oxidize the organic compounds to CO_2 and H_2O. As a consequence, the enhanced charge separation and transfer induces the superior photocatalytic activity of the heterostructured ZnO NPs/mesoporous anatase–TiO_2 (B) biphase TiO_2 nanowires heterojunction.

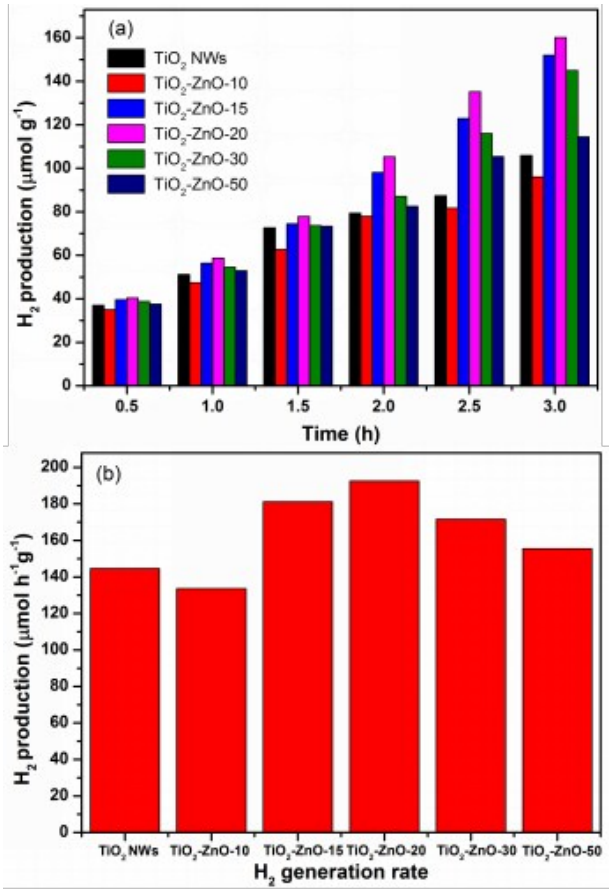

Fig. 10. H_2 evolution from water splitting over TiO_2 NWs, and TiO_2-ZnO samples by using methanol as an electron donor.

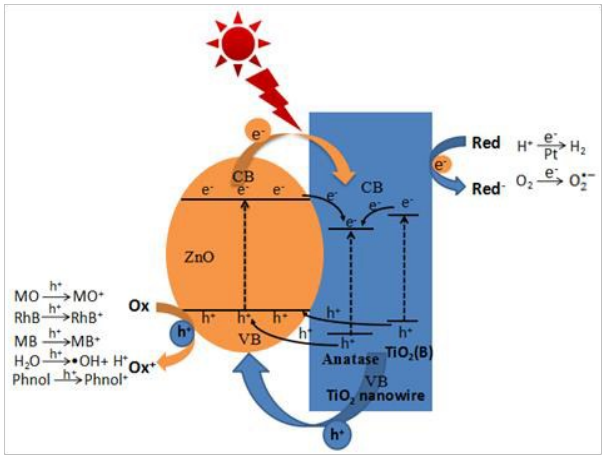

Fig. 11. Schematic illustration of photo-induced charge transfer and separation at the interface of TiO_2-ZnO heterostructure.

4. Conclusions

In this work, we developed a simple solution synthesis method to prepare a heterojunction photocatalyst of ZnO NPs decorating biphase TiO_2 NWs. The as-prepared TiO_2-ZnO hybrid presents appreciable photocatalytic performance in pollutant degradation as well as H_2 evolution, which can be mainly attributed to their constructed wire-like morphology, multiphase structure, high BET surface area, and heterojunction built. It is promising that this material can be further used in the fields of rechargeable lithium-ion batteries, gas sensors, and electrodes in solar cells.

Acknowledgements

This work was financially supported by the National Natural Science Foundation of China (No.21667019), the Key Project of Natural Science Foundation of Jiangxi Province (No.20171ACB20016), the Jiangxi Province Major Academic and Technical Leaders Cultivating Object Program (No.20172BCB22014), the Key Laboratory of Photochemical Conversion and Optoelectronic Materials, TIPC, CSA (No.PCOM201401) and Key Project of Science and Technology Research of Jiangxi Provincial Department of Education (No.DA201602063). Financial support for this work was further provided by the Fundamental Research Funds for the Central Universities (112109*172210171), the Start-up Foundation for Hundred-Talent Program of Zhejiang University (112100-193820101/001/022), and National Natural Science Foundation of China (No.51702284).

Supporting Information

Supplementary data associated with this article can be found, in the online version.

References

[1] J. Zhao, Q. Lu, C. Wang and S. Liu, *Journal of Nanoparticle Research*, 2015, 17, 189.
[2] X. Liu, J. Chen, P. Liu, H. Liu, G. Li, T. An and H, Zhao, *Applied Catalysis A: General*, 2016, 521, 34-41.
[3] L. Z. Wu, B. Chen, Z. J. Li, C. H. Tung, Accounts of Chemical Research, 2014, 47, 2177-2185.
[4] J. Jia, D. Li, J. Wan, and X. Yu, *Journal of Industrial and Engineering Chemistry*, 2016, 33, 162-169.
[5] M. D. Regulacio and M.-Y. Han, *Accounts of chemical research*, 2016, 49, 511-519.
[6] S. Das, H. Sopha, M. Krbal, R. Zazpe, V. Podzemna, J. Prikryl and J. M. Macak, *ChemElectroChem*, 2017, 4, 495-499.
[7] M. Kawa, A. Podborska and K. Szaciłowski, *Journal of Physics: Conference Series*, 2016, 745, 032102.
[8] M. M. Momeni and Y. Ghayeb, *Applied Physics A*, 2016, 122, 620.
[9] W. Yin, W. Wang and S. Sun, *Catalysis Communications*, 2010, 11, 647-650.
[10] W.-T. Chen, A. Chan, D. Sun-Waterhouse, T. Moriga, H. Idriss and G. I.N. Waterhouse, *Journal of Catalysis*, 2015, 326, 43-53.
[11] L. Qi, B. Cheng, J. Yu and W. Ho, *Journal of Hazard Mater*, 2016, 301, 522-530.

[12] K. Tahir, A. Ahmad, B. Li, S. Nazir, A.U. Khan, T. Nasir, Z.U. Khan, R. Naz and M. Raza, *Journal of Photochemistry and Photobiology B: Biology*, 2016, 162, 189-198.
[13] R. M. Kulkarni, R. S. Malladi, M. S. Hanagadakar, M. R. Doddamani, B. Santhakumari and S. D. Kulkarni, *Journal of Materials Science*: *Materials in Electronics*, 2016, 27, 13065-13074.
[14] P. S. Pillai, D. I. Prajapati, R. Ameta and Y. Ali, *Scientific Reviews and Chemical Communications*, 2016, 6, 12-18.
[15] S. Horikoshi, Y. Shirasaka, H. Uchida, N. Horikoshi and N. Serpone, *Photochemical & Photobiological Sciences*, 2016, 15, 1061-1070.
[16] Y.-H. Lin, H.-T. Hsueh, C.-W. Chang and H. Chu, *Applied Catalysis B: Environmental*, 2016, 199, 1-10.
[17] C. Xue, W. Wang, T. Han, Y. Wang, Y. Dong, S. Hu and J. Yang, *Chemistry Letters*, 2016, 45, 1460-1462.
[18] L. Wu, H. Zhao, L. Jin and H. Xu, *Frontiers of Materials Science*, 2016, 10, 310-319.
[19] S. Khanchandani, S. Kumar and A.K. Ganguli, *ACS Sustainable Chemistry & Engineering*, 2016, 4, 1487-1499.
[20] L. Wang, X. Duan, G. Wang, C. Liu, S. Luo, S. Zhang, Y. Zeng, Y. Xu, Y. Liu and X. Duan, Applied Catalysis B: Environmental, 2016, 186, 88-96.
[21] C. Liu, L. Wang, Y. Tang, S. Luo, Y. Liu, S. Zhang, Y. Zeng and Y. Xu, Applied Catalysis B: Environmental, 2015, 164, 1-9.
[22] L. Wang, X. Liu, J. Luo, X. Duan, J. Crittenden, S. Zhang, Y. Pei, Y. Zeng and X. Duan, Angewandte Chemie International Edition, 2017, 56, 7610-7614.
[23] X. B. Li, Y. J. Gao, Y. Wang, F. Zhan, X. Y. Zhang, Q. Y. Kong, N. J. Zhao, Q. Guo, H. L. Wu, Z. J. Li, Y. Tao, J. P. Zhang, B. Chen, C. H. Tung ang L. Z. Wu, *Journal of the American Chemical Society*, 2017, 139, 4789-4796.
[24] A. Muzakki, H. Shabrany and R. Saleh, *AIP Conference Proceedings*, 2016, 1725, 020051.
[25] V. Lachom, P. Poolcharuansin and P. Laokul, *Materials Research Express*, 2017, 4, 035006.
[26] R. Vinoth, P. Karthik, K. Devan, B. Neppolian and M. Ashokkumar, *Ultrason Sonochem*, 2017, 35, 655-663.
[27] X. Guan, J. Shi, L. Guo, *International Journal of Hydrogen Energy*, 2013, 38, 11870-11877.
[28] L. Roza, M.Y.A. Rahman, A.A. Umar and M.M. Salleh, *Journal of Alloys and Compounds,* 2015, 618, 153-158.
[29] J. Saffari, N. Mir, D. Ghanbari, K. Khandan-Barani, A. Hassanabadi and M. R. Hosseini-Tabatabaei, *Journal of Materials Science: Materials in Electronics*, 2015, 26, 9591-9599.
[30] L. Hou, L. Lian, L. Zhang, G. Pang, C. Yuan and X. Zhang, *Advanced Functional Materials*, 2015, 25, 238-246.
[31] R. K. Sonker, S. R. Sabhajeet, S. Singh and B. C. Yadav, *Materials Letters*, 2015, 152, 189-191.
[32] B. Siwach, S. Sharma and D. Mohan, *Journal of Integrated Science & Technology*, 2017, 5, 1-4.
[33] S. Rehman, R. Ullah, A. M. Butt and N. D. Gohar, *Journal of hazardous materials*, 2009, 170, 560-569.
[34] X. Yan, C. Zou, X. Gao, W. Gao, *Journal of Materials Chemistry*, 2012, 22, 5629-5640.
[35] Q. Hu, Y. Li, F. Huang, Z. Zhang, K. Ding, M. Wei and Z. Lin, *Scientific Reports,* 2015, 5, 11499.
[36] L. Pan, G. Shen, J. Zhang, X. Wei, L. Wang, J. Zou and X. Zhang, *Industrial & Engineering Chemistry Research*, 2015, 54, 7226-7232.
[37] S. Iijima, *Nature*, 1991, 354, 56.
[38] M. Ge, C. Cao, J. Huang, S. Li, Z. Chen, K. Zhang, S. S. Al-Deyab and Y. Lai, *Journal of Material Chemistry A*, 2016, 4, 6772-6801.
[39] G. Wang, H. Wang, Y. Ling, Y. Tang, X. Yang, R. C. Fitzmorris, C. Wang, J. Z. Zhang and Y. Li, *Nano Letters*, 2011, 11, 3026-3033.
[40] X. Zhang, J. Pan, A. J. Du, P. F. Lee, D. D. Sun and J. O. Leckie, *Chemistry Letters*, 2008, 37, 424-425.
[41] R. Marchand, L. Brohan and M. Tournoux, *Materials Research Bulletin*, 1980, 15, 1129-1133.
[42] G. Wang, Q. Wang, W. Lu and J. Li, *The Journal of Physical Chemistry B*, 2006, 110, 22029-22034.
[43] B. Liu, A. Khare and E. S. Aydil, *ACS applied materials & interfaces*, 2011, 3, 4444-4450.
[44] L. Shen, Z. Xing, J. Zou, Z. Li, X. Wu, Y. Zhang, Q. Zhu, S. Yang and W. Zhou, *Scientific Reports*, 2017, 7, 41978.
[45] D.C. Hurum, A.G. Agrios and K.A. Gray, *The Journal of Physical Chemistry B*, 2003, 107, 4545-4549.
[46] W. Li, C. Liu, Y. Zhou, Y. Bai, X. Feng, Z. Yang, L. Lu, X. Lu and K.-Y. Chan, *The Journal of Physical Chemistry C*, 2008, 112, 20539-20545.
[47] D. Yang, H. Liu, Z. Zheng, Y. Yuan, J C. Zhao, E. R. Waclawik, X. Ke and H. Zhu, *Journal of the American Chemical Society*, 2009, 131, 17885-17893.
[48] H.-H. Lo, N. O. Gopal, S. C. Sheu and S. C. Ke, *The Journal of Physical Chemistry C*, 2014, 118, 2877-2884.
[49] W. Zhou, L. Gai, P. Hu, J. Cui, X. Liu, D. Wang, G. Li, H. Jiang, D. Liu, H. Liu and J. Wang, *CrystEngComm*, 2011, 13, 6643-6649.
[50] T. Beuvier, M. Richard-Plouet and L. Brohan, *The Journal of Physical Chemistry C*, 2009, 113, 13703-13706.
[51] M. Ebrahimian, R. Soroush, A. Y. Salekdeh, M. Abazaril, A. Langari, M. G. H. Kharaji. *World Applied Sciences Journal*, 2012, 19, 1602-1606.
[52] Q. Zhang, W. Fan and L. Gao, *Applied Catalysis B: Environmental*, 2007, 76, 168-173.
[53] S. Chen, H. Zhang, X. Yu, W. Liu, J. Wang, Q. Liu and L. Chen, *Materials Chemistry and Physics*, 2010, 124, 1057-1064.
[54] E. Liu, L. Kang, F. Wu, T. Sun, X. Hu, Y. Yang, H. Liu and J. Fan, *Plasmonics*, 2013, 9, 61-70.

View Article Online
DOI: 10.1039/C7TA10274G

Table of contents entry

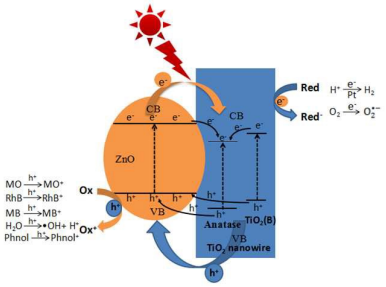

A novel ZnO NPs / mesoporous anatase−TiO_2 (B) NWs heterojunction photocatalyst was synthesized for environmental purification and hydrogen evolution.